System Impact of Laser Phase Noise On 400G And Beyond Coherent Pluggables

Hai Xu[1], Marcos Olmos Rebellato[2], Shih-Cheng Wang[1]
[1]Marvell Technology, Inc., 5488 Marvell Lane, Santa Clara, CA 95054, USA
[2]Marvell Technology, Inc., Humberto Primo 680, Piso 6, Oficina 66, Edificio Suquia, Complejo Capitalinas, Cordoba X5000FAN, Argentina
xhai@marvell.com

Abstract: We show that 800G systems are highly sensitive to phase noise of local oscillator. We introduce a PI model that correlates well with measured performance. We present performance simulations and limitations of current timing recovery. © 2022 The Author(s)

1. Introduction

It is well known that the phase noise of the local oscillator (LO) plays an important role on the performance of advanced optical coherent system, particularly in the presence of chromatic dispersion [1]. Electric dispersion compensation (EDC) induces a penalty known as equalization enhanced phase noise (EEPN), in two ways: extra inter-symbol interference (ISI) noise induced by phase noise spread [1-3] and timing jitter converted from frequency noise [3, 4]. In this paper, we will study its impact on 400G and beyond coherent pluggable modules. And we will discuss using simulations new challenges due to the bursty nature of frequency noise. We also develop a PI model to evaluate this system impact directly from measurement of laser phase noise, and therefore save the efforts of sophisticated system implementation/simulation. Note that in this work we concentrate on single-carrier signals. Sub-carrier multiplexing is more robust to EEPN but may require more R&D to reduce power and cost.

2. Measurement of laser noise and 400G System performance

In this measurement we focused on three commercial Integrable Tunable Laser Assemblies (ITLA), and we called them 1, 2, and 3. We used a coherent receiver including a high-quality tunable laser as LO, a hybrid, balanced detectors, and a high-speed real-time scope to measure the frequency noise spectra of these ITLAs. The linewidth of the LO is specified below 100 Hz. A polarization controller was inserted before the coherent receiver to maximize the received power at the measured polarization. The frequency power spectral density (PSD) was calculated from I and Q waveforms on the scope [5]. The scope sampling frequency was 20 GHz, and the length of each capture was 500K (25 µs). We took 400 captures for each ITLA. The average and maximum of noise spectra are shown in Fig. 1. As shown in Fig. 1(A), the average linewidths of the lasers are 10.5, 126.7, and 288.3 KHz respectively. In the meantime, as shown in Fig .1(B), ITLA-3 can emit significantly higher than average noise during certain 25-µs time windows. For these worst noise cases, the linewidths were calculated to 11.2, 128.1, 320.4 KHz. Correspondingly, one would expect the system performance will fluctuate over different 25-µs time periods, particularly for ITLA-3. By comparison, the noise spectrum obtained with a spectrum analyzer measures the average spectrum and therefore the result may not disclose the worst case.

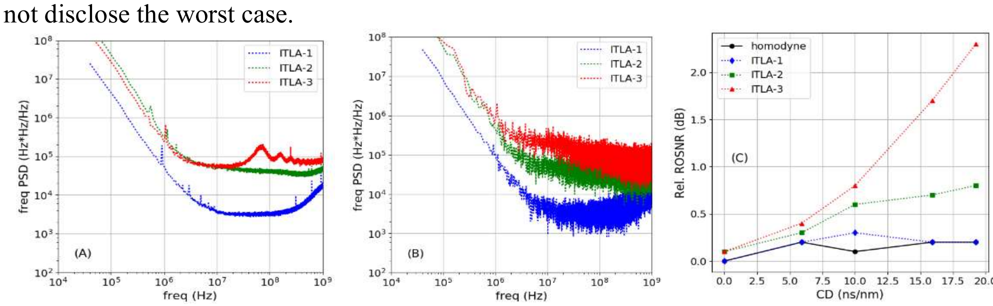

Fig. 1. Frequency noise spectra (A) average and (B) maximum from 400 captures. (C) The relative received optical signal-to-noise ratio (ROSNR)

Next, using these three ITLAs as LO we measured 400G system performance in the presence of chromatic dispersion (CD). The Marvell Deneb DSP chip is used as data source and DSP receiver. With openFEC (OFEC) implemented, the baud rate is 63.14 GBds for QAM16 and the FEC threshold is specified at 0.02 for ideal AWGN. The signal was sent via a commercial Class-40 coherent driver modulator (CDM) and received by a commercial Class-40 integrated coherent receiver (ICR). The laser at the transmitter is another ITLA with similar quality as ITLA-1. A CD emulator and an ASE source were used to adjust link CD and OSNR. In this measurement, Deneb is set to collect pre-FEC and post-FEC BER over 1 minute. In Fig. 1(C) we show the ROSNR penalty from a homodyne back-to-back case, in which tens of meters of fiber were used to decorrelate the phase between TX and RX. The phase noise itself was well recovered by the DSP for all three lasers, as shown by the small performance penalty when CD is small. However, when CD increases, EEPN became significant and the induced ROSNR penalty was as high as 0.8 and 2.4 dB for ITLA-2 and 3 at 20 ns/nm. By comparison, the ITLA-1 show the best performance and maintains the ROSNR around 0.2 dB. The large penalty of ITLA-3 is mainly from burst errors. For example, at CD of 20 ns/nm, the FEC was broken at pre-FEC BER of 1.81e-2, 1.73e-2, and 1.16e-2 for ITLA-1, 2, and 3, respectively. This behavior echoes the large variation in measured PSD for ITLA-3 in Fig. 1(B).

3. Simulation of 400G and beyond

In this section, we investigated 400G and beyond using Marvell's floating-point simulation model of the next-generation DSP. The simulator simulates the exact procedure and parameters of the chip, including realistic ADC/DAC and PLL. We adopted design parameters of 400G and 800G CDM and ICR from commercial vendors. Again, we focused on OFEC. We used baud rate of 64 GBds and 128 GBds. Note that these baud rates were used for easy comparison, and they are slightly different from the exact OFEC baud rate. At the transmitter laser, no phase noise was added. The above experimentally captured phase waveforms were added in the LO. We also used LO without phase noise as baseline, called "Ref". In the simulation, we collected 15M symbols under various levels of OSNR. ROSNR was referred to as the OSNR level that pre-FEC BER reached 0.02. In Fig. 2 we show the ROSNR relative to the case of "Ref". In (A) the pre-FEC BER used in the ROSNR calculation is average BER of the entire 15M symbols while in (B) we divided the 15M symbols into segments, each containing 172k bits ─ the interleaving length of OFEC, and pre-FEC BER was the maximum BER among these segments. In the FEC decoder, if pre-FEC BER within the interleaving length exceed the FEC threshold, post-FEC error will occur.

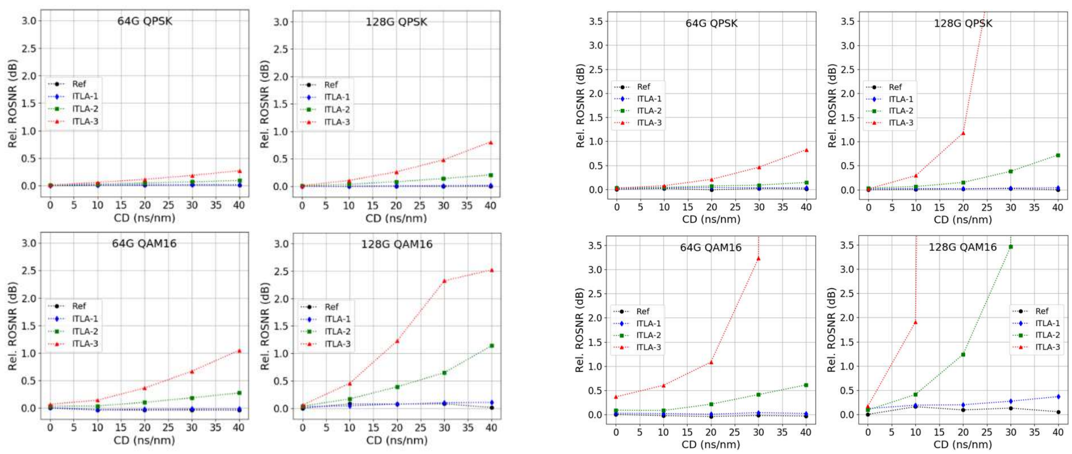

(A) (B)

Fig. 2. Relative RONSR penalty based on pre-FEC BER = 0.02 with pre-FEC BER was used with average (A) and maximum (B) from 15M symbols. The baud rate and modulation format are described in subtitle.

In Fig. 2(A), for 400G QAM16 and CD of 20 ns/nm, there is only 0.4 dB penalty from ITLA-3, which strongly disagrees with the experimental observation shown in Fig. 1. When maximum pre-FEC BER is used in Fig. 2(B), the penalty increased to 1.05 dB, showing a better agreement. But there was still a 1.4 dB gap from observed 2.4-dB penalty, and we believe 15M symbols (234 µs) is still too short to accurately represent the bursty nature of the phase noise. As a result, when studying the system impact of EEPN, we will face new challenges: Simulations reporting average pre-FEC BER will underestimate performance degradations. In order to accurately monitor the FEC breaking events, one needs to calculate the maximum BER from segments of interleaving length or implement a FEC decoder. Moreover, a sufficiently large number of symbols is required to catch the burst events in the laser phase noise. From another perspective, this also suggests that FEC with interleaving length longer than 172k bits might be more robust against EEPN. In a similar experiment as Sect. 2, Marvell DSP chip Canopus, equipped with a FEC of interleaving length around 500k, did see better tolerance.

Despite of the limitation in the simulations, the system impact from EEPN is qualitatively shown in Fig. 2(B). ITLA-1 is still working for 800G (128G QAM16) while ITLA-2 reached 20 ns/nm with penalty of 1.3-dB penalty. But ITLA-3 induced 2 dB penalty at 10 ns/nm and cannot converge at 20 ns/nm and more. For 400G, 128G QPSK show similar EEPN penalty as 64G QAM16 except that ITLA-3 show 0.3-dB B2B penalty in QAM16.

4. PI model

To study the system impact of EEPN induced timing error at a more fundamental level, we need to understand the transfer function from EEPN induced timing drift to the residual timing error received by the decision circuit. The timing recovery in the DSP is commonly implemented with a feedback process: The timing error is obtained from the signal at a stage after the timing adjusting circuit, for example, the output of phase recovery in the Mueller-Müller method [6] or the output of the timing recovery circuit in the Gardner method [7]. This timing error is then fed back to the timing recovery to adjust the timing of later signals, after a certain latency, necessitated by the circuit design. This feedback process can be described by proportional-integral (PI) filter model [8], where signal timing is adjusted by the timing error following:

$$u(t) = k_p e(t) + k_i \int e(\tau) dt \qquad (1)$$

In Eq. (1), $u(t)$ is the timing adjustment and $e(t)$ is detected timing error. The proportional and integral gain are represented by k_p and k_i respectively. For a DSP chip with parallelism of p and latency of n parallelism, we can derive the Laplace transfer function from EEPN generated timing error to residual timing error at the output of timing recovery, i.e., the timing error seen by decision circuit, as:

$$\mathrm{G(s)} = \frac{\mathrm{e^{-snpT}(k_p s + k_i)}}{\mathrm{e^{-snpT}(k_p s + k_i) + s - s e^{-spT}}} \qquad (2)$$

where T is the symbol period. In practice, parallelism in advanced high-speed DSPs is in the range of 50-200 symbols.

Extending the simulation in sect. 3, we correlated the magnitude of error vectors with residual timing error calculated from Eq. (2). From simulation, we calculated EVM_{RMS}[9] from various parallelism of symbols. For each parallelism, we then calculated the EEPN timing error from laser phase added at the LO for this parallelism and use Eq. (2) to get the residual timing error. The correlation results are shown in Fig. 3.

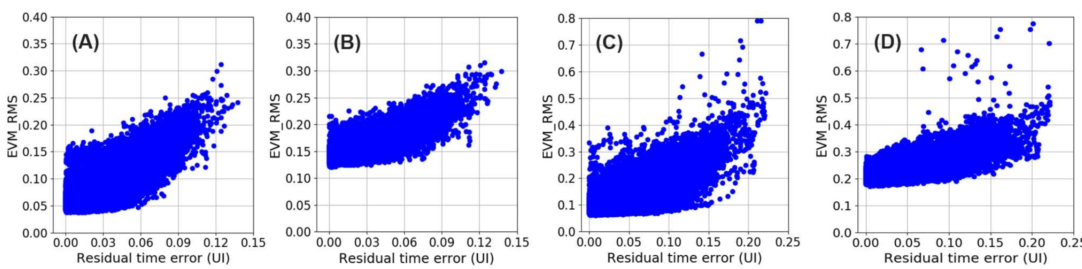

Fig. 3. EVM v.s. residual timing error from PI for (A) 64GBds QAM16 without ASE, (B) 64GBds QAM16 at OSNR 25 dB, (C) 128 GBds QAM16 without ASE, and (D) 128 GBds QAM16 at OSNR 25 dB

Good correlation was achieved. The outliers in the 128 GBds cases were due to cycle slips. The EVM increased proportionally with the calculated timing error. Therefore, from the measured laser phase, we can identify the moments when the performance was degraded. Furthermore, the EVM when the residual time error is near zero may indicate the strength of the "noise" part of EEPN. Finally, we tried varying parameters in PI and the results show that the capability of a feed-back based timing recovery to recover EEPN induced timing jitter is limited. A feed-forward process may be considered.

In summary, we discussed the system impact of EEPN at 400G and beyond. We show that the tolerance for EEPN is tighter for 800G. FEC with long interleaving will help. With EEPN, one needs long simulation length to catch the bursty behavior. A PI model was proposed to estimate the system impact directly from laser phase waveform.

5. References

[1] Shieh and K. P. Ho, "Equalization-enhanced phase noise for coherent detection systems using electronic digital signal processing," Opt. Exp., **16**, 15718–15727, (2008).
[2] S. Oda, "Interplay Between Local Oscillator Phase Noise and Electrical Chromatic Dispersion Compensation in Digital Coherent Transmission System", ECOC 2010, Sept 2010
[3] Kakkar, A., Rodrigo Navarro, J., Schatz, R. et al. "Laser Frequency Noise in Coherent Optical Systems: Spectral Regimes and Impairments," Nature Sci Rep 7, 844 (2017)
[4] H. Sun and K-T Wu, "Clock recovery and jitter sources in coherent transmission systems", OFC 2012, March 2012
[5] R. Maher and B. Thomsen, "Dynamic linewidth measurement technique using digital intradyne coherent receivers," Opt. Exp., **19**, B313–B322, (2011).
[6] K. H. Mueller and M. Müller, "Timing recovery in digital synchronous data receivers," IEEE Tans. Commun., **24**, 516–531, 1976.
[7] F. M. Gardner, "A BPSK/QPSK timing-error detector for sampled receivers," IEEE Tans. Commun., **34**, 423–429, May 1986
[8] Brosilow, C. and Joseph, B. (2002). Techniques of Model-Based Control. Prentice-Hall. New Jersey
[9] Implementation Agreement 400ZR, OIF-400ZR-01.0, OIF Forum, March 2020. Available: https://www.standards.govt.nz/search-and-buy-standards/standards-information/quality-management-systems/